Cell Reports

Article

Calreticulin mutations affect its chaperone function and perturb the glycoproteome

Graphical abstract

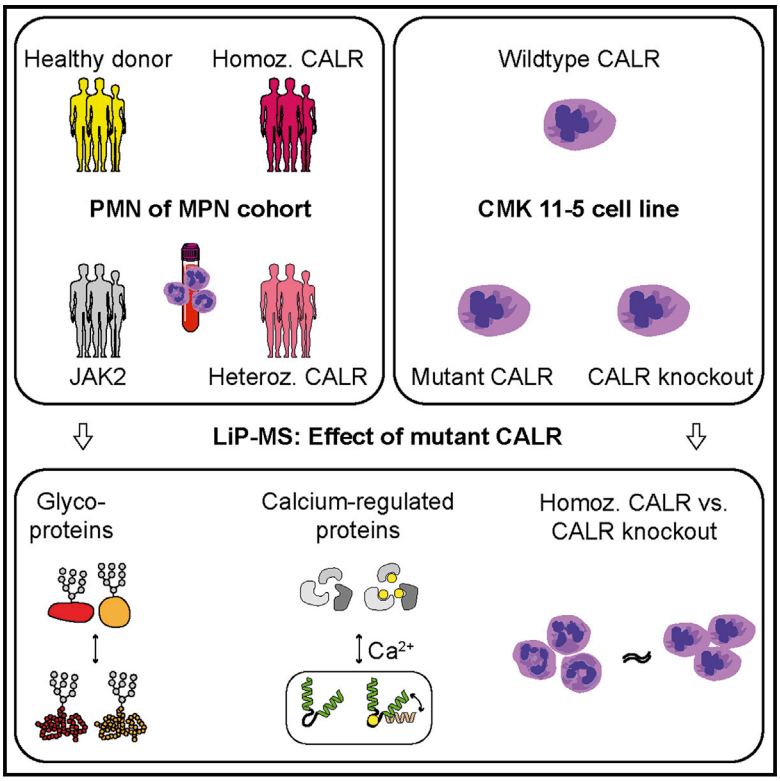

Authors

Patrick M. Schürch, Liliana Malinovska, Mohammad Hleihil, ..., Bernd Wollscheid, Paola Picotti, Alexandre P.A. Theocharides

Correspondence

alexandre.theocharides@usz.ch

In brief

Schürch et al. apply limited proteolysis-coupled mass spectrometry to assess structural perturbations of the proteome in myeloproliferative neoplasms (MPNs) with mutations in the endoplasmic reticulum chaperone calreticulin. They show that *calreticulin* mutations perturb the structural landscape of the glycoproteome and provide molecular proof of protein misfolding in *calreticulin*-mutated MPNs.

Highlights

- Proteolysis-coupled mass spectrometry analysis of myeloproliferative neoplasms
- Homozygous *CALR* mutations perturb the structural landscape of the glycoproteome
- *CALR* mutations lead to a chaperone defect and misfolding of myeloperoxidase
- Both the holdase and foldase functions are affected by *CALR* mutations

Schürch et al., 2022, Cell Reports *41*, 111689
November 22, 2022
https://doi.org/10.1016/j.celrep.2022.111689

CellPress

Cell Reports

CellPress
OPEN ACCESS

Article

Calreticulin mutations affect its chaperone function and perturb the glycoproteome

Patrick M. Schürch,[1] Liliana Malinovska,[2] Mohammad Hleihil,[3] Marco Losa,[4] Mara C. Hofstetter,[1] Mattheus H.E. Wildschut,[1,2,5] Veronika Lysenko,[1] Asvin K.K. Lakkaraju,[4] Christina A. Maat,[2] Dietmar Benke,[3] Adriano Aguzzi,[4] Bernd Wollscheid,[5,6] Paola Picotti,[2] and Alexandre P.A. Theocharides[1,7,*]

[1]Department of Medical Oncology and Hematology, University of Zurich and University Hospital Zurich, Raemistrasse 100, 8091 Zurich, Switzerland
[2]Institute of Molecular Systems Biology (IMSB), Department of Biology, ETH Zurich, Zurich, Switzerland
[3]Institute of Pharmacology and Toxicology, University of Zurich, Zurich, Switzerland
[4]Institute of Neuropathology, University Hospital Zurich, Zurich, Switzerland
[5]Institute of Translational Medicine (ITM), Department of Health Sciences and Technology, ETH Zurich, Zurich, Switzerland
[6]Swiss Institute of Bioinformatics (SIB), Lausanne, Switzerland
[7]Lead contact
*Correspondence: alexandre.theocharides@usz.ch
https://doi.org/10.1016/j.celrep.2022.111689

SUMMARY

Calreticulin (CALR) is an endoplasmic reticulum (ER)-retained chaperone that assists glycoproteins in obtaining their structure. *CALR* mutations occur in patients with myeloproliferative neoplasms (MPNs), and the ER retention of CALR mutants (CALR MUT) is reduced due to a lacking KDEL sequence. Here, we investigate the impact of *CALR* mutations on protein structure and protein levels in MPNs by subjecting primary patient samples and *CALR*-mutated cell lines to limited proteolysis-coupled mass spectrometry (LiP-MS). Especially glycoproteins are differentially expressed and undergo profound structural alterations in granulocytes and cell lines with homozygous, but not with heterozygous, *CALR* mutations. Furthermore, homozygous *CALR* mutations and loss of CALR equally perturb glycoprotein integrity, suggesting that loss-of-function attributes of mutated CALR chaperones (CALR MUT) lead to glycoprotein maturation defects. Finally, by investigating the misfolding of the CALR glycoprotein client myeloperoxidase (MPO), we provide molecular proof of protein misfolding in the presence of homozygous *CALR* mutations.

INTRODUCTION

Myeloproliferative neoplasms (MPNs) comprise essential thrombocythemia (ET), polycythemia vera (PV), and myelofibrosis (MF).[2] MPNs are characterized by cytokine-independent activation of the Janus kinase-signal transducer and activator of transcription (JAK-STAT) signaling pathway. MPN-associated driver mutations typically hyperactivate the Janus kinase 2 (*JAK2*) or the upstream thrombopoietin receptor. Moreover, calreticulin (*CALR*) mutations give rise to mutated CALR chaperones (CALR MUT), which induce thrombopoietin-receptor-mediated signaling.[3] Approximately 20%–30% of patients with ET and MF carry insertion/deletion *CALR* mutations, of which 80% exhibit either a type 1 (T1) or a T2 mutation.[4–6] To date, JAK-STAT-signaling-independent effects of *CALR* mutations remain underexplored. CALR is a vital calcium buffer and, as a chaperone, aids glycoproteins in obtaining their mature structure, which allows proper function.[7–9] CALR acts as a holdase that preferentially binds glycosylated precursors via its N-terminal lectin domain and binds to non-glycosylated proteins, thereby preventing the aggregation, premature oligomerization, oxidation, and degradation of unfolded proteins.[10–14] During chaperoning, the CALR P-domain serves as a docking site for foldases like peptidyl-prolyl *cis-trans* isomerase (CYPB) or protein disulfide isomerase A3 (PDIA3 or ERp57), which ensure proper reshuffling of proline residues or disulfide bonds of the client glycoprotein.[15] The various insertion/deletion *CALR* mutations lead to a +1 frameshift that generates a conserved mutant-specific C terminus. The mutant C terminus alters the biochemical properties of CALR MUT by promoting CALR MUT multimer formation and increasing the lectin-mediated affinity of CALR MUT to the thrombopoietin receptor, which consequently promotes thrombopoietin receptor dimerization and cytokine-independent JAK-STAT signaling.[3,16–18] In addition, calcium-binding stretches are lost in *CALR* T1 mutations, leading to impaired calcium buffering in *CALR*-mutated cells.[6,19] In primary megakaryocytes, a defective association of CALR MUT with the store-operated calcium entry complex leads to uncontrolled calcium fluxes into the cytosol.[19] Furthermore, the C terminus lacks the KDEL sequence, leading to reduced endoplasmic reticulum (ER) retention of CALR MUT.[20] Recent studies suggest that protein folding might be affected in *CALR*-mutated cells; one study suggested that *CALR* mutations lead to an upregulation of the unfolded protein response (UPR), whereas another

study reported an impaired UPR response in *CALR*-mutated cells.[21,22] Furthermore, patients with homozygous *CALR* mutations develop a myeloperoxidase (MPO) glycoprotein deficiency. The MPO deficiency is characterized by the loss of protein expression due to premature proteasomal degradation, but whether this is a direct cause of a chaperone defect remains to be determined.[23] Similarly, human embryonic kidney cells expressing CALR MUT solely exhibited a compromised major histocompatibility complex (MHC) class I glycoprotein maturation and partially reduced MHC class I levels.[24]

To date, the impact of *CALR* mutations on chaperone function remains unclear. Since protein function is tightly linked to the structural integrity of the folded polypeptide chain, we analyzed primary *CALR*-mutated granulocytes with the recently developed limited proteolysis-coupled mass spectrometry (LiP-MS) workflow. LiP-MS is a technology that simultaneously probes for protein-level changes and altered *in situ* structure-specific proteolytic patterns between different proteotypes.[25–28] More precisely, exposure or masking of LiP protease cleaving sites by structural changes, but also other effects (e.g., altered protein-protein interactions) dictate the proteolytic patterns. By characterizing the conformational landscape and protein abundance profile of patient-derived ET and MF granulocytes and comparing them with healthy blood donors, we show that perturbations to glycoprotein integrity requires mutations on both *CALR* alleles. In addition, mutant CALR differentially affected protein groups, with certain perturbations being only detectable on a structural level. Furthermore, to follow up on the structurally most altered protein from our screen, we further elucidated the mechanism of MPO deficiency. Our data demonstrate that apart from a quantitative CALR chaperone defect caused by CALR MUT secretion, *CALR* mutations also qualitatively affect CALR MUT chaperone function by interfering with glycoprotein and co-chaperone binding. This study demonstrates the applicability of LiP-MS for primary patient samples and increases the knowledge of the impact of *CALR* mutations on CALR function. Our findings also contribute to a deeper understanding of homozygous *CALR* mutations, which have been associated with disease progression.[29,30]

RESULTS

LiP-MS detects proteomic perturbations in MPN granulocytes with a homozygous *CALR* mutation

We aimed at investigating the *in situ* impact of CALR MUT on glycoproteins and other protein groups. Therefore, we tested the ability of LiP-MS to assess proteome-wide alterations in protein abundance and conformations in primary granulocyte of patients with *CALR*-mutated MF and ET (Figure 1A; Table 1). Overall, we quantified abundance changes of 1,090 granulocytic proteins (Figure 1B). In addition, we detected 13,091 altered peptides, which enabled probing the structural features of 1,837 granulocytic proteins, respectively.

We first compared the proteotypes between patients and healthy donors (HDs). The extent of proteins with altered abundance and/or structural perturbations in patients with heterozygous *CALR* mutations was low and comparable to patients with *JAK2* mutations (Figure 1B). In contrast, patients with homozygous *CALR* mutations showed marked alterations in protein abundance (64 proteins, 2.2% of detected proteomes) and structural alterations (118 proteins, 4%) or both (30 proteins, 1%) (Figure 1B; Table S1). Moreover, we detected various MPO-derived structurally altered peptides in patients with homozygous, but not heterozygous, *CALR* mutations, which is in line with previous observations (Figure 1C).[23] Based on the molecular functions of CALR, we next grouped the affected proteins into glycoproteins, non-glycosylated and calcium-regulated/related proteins, or neither of both (OTHER). The overlap between altered protein abundance levels and structural alterations was low between patients with hetero- and homozygous *CALR* mutations (Figures 1D and 1E). This suggests that certain cellular processes are only affected by homozygous, but not by heterozygous, *CALR* mutations. In summary, LiP-MS can reliably detect predicted structural perturbations in patient-derived samples, and extensive proteome perturbations occur mainly in the homozygous *CALR*-mutated state.

Gene ontology enrichment analysis reveals that homozygous *CALR* mutations perturb the glycoproteome and differentially affect protein subclasses

Since patients with homozygous *CALR* mutations showed the strongest proteomic perturbations, we further pursued our analysis on these patients in order to gain insights on the consequences of *CALR* mutations for CALR function. In line with previous reports, we observed a consistent upregulation of UPR effectors, which is indicative of protein misfolding (Figure S1A).[21,22] To determine the proteins impacted by *CALR* mutations, we performed a Gene Ontology (GO) enrichment analysis of the proteins with abundance changes and/or structural changes occurring in the proteomes of patients with homozygous *CALR* mutations versus *JAK2*-mutated controls (Table S2). Glycoproteins (GO term "glycoprotein"), which are chaperoned by CALR, enriched for structural and abundance level changes (Figures 2A and 2B). This was paralleled by an enrichment of disulfide-bond-containing proteins (GO term "disulfide bond"), of which 69.6% were glycoproteins that naturally require reshuffling of disulfide bonds by foldases (Figure 2C). Furthermore, the majority of glycoproteins with structural alterations exhibited reduced abundance levels (48.9%) (Figure 2D). This further supports a CALR chaperone defect resulting in the degradation of disulfide-bridge-containing glycoprotein clients in the presence of homozygous *CALR* mutations. Structural perturbations also enriched in calcium-regulated proteins (GO term "calcium"), but, in contrast to glycoproteins, *CALR* mutations affected 67% of calcium-regulated proteins, mainly on a structural level, without significant changes in protein abundance (Figures 2A and 2D). LiP-MS also detected changes occurring exclusively on a structural level in several of the remaining proteins groups. These groups included cytoskeletal proteins and ubiquitin-pathway-related proteins (Figure 2C). Taken together, LiP-MS was able to capture the consequences of homozygous *CALR* mutations on protein structure and abundance levels of protein groups.

In order to elucidate whether the proteome perturbations observed in patients with a homozygous *CALR* mutation also occur in the heterozygous state, we next searched for similarities between the proteomes of patients with hetero- and homozygous *CALR* mutations by comparing the

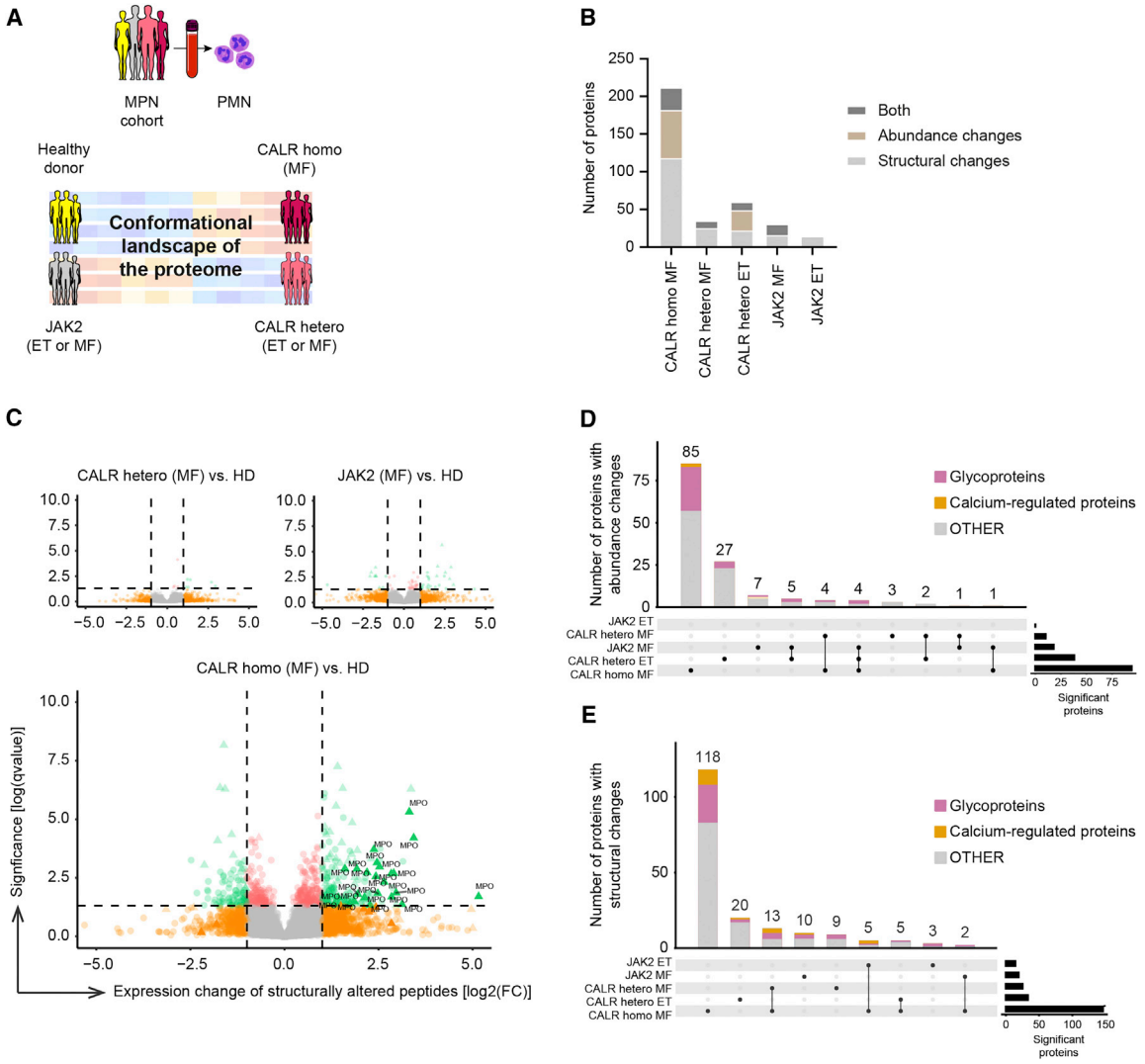

Figure 1. LiP-MS detects proteomic perturbations in MPN granulocytes with a homozygous *CALR* mutation

(A) Overview of patient and healthy donor (HD) samples investigated in the study. Proteomes of primary peripheral blood-derived polymorphonuclear cells (PMNs) from patients with *JAK2*- and *CALR*-mutated ET/MF and age-matched HDs were subjected to LiP-MS.

(B) Number of proteins with altered expression levels and/or structural changes in hetero- or homozygous patients with *CALR*- and *JAK2*-mutated ET/MF compared with HDs.

(C) Conformational alterations detected in the proteomes of hetero- or homozygous patients with *CALR*-mutated and *JAK2*-mutated MF compared with HDs. Volcano plots show log2(fold change) (FC) of structurally altered peptides versus log of adjusted p value (q value). FCs of the structurally altered peptides were normalized to a significant (triangles) or non-significant (spheres) log2(FC) of the underlying protein. The color code indicates whether the log2(FC) of the structurally altered peptide is significant (green), non-significant (gray), or did not reach the q-value cutoff (red) or the log2(FC) cutoff (orange). MPO-derived peptides are indicated.

(D and E) Number of proteins with altered abundance (D) or structural changes (E) when the proteomes of patients are compared with HD controls. Dots indicate the patient group that was compared with HDs, whereas lines connecting the dots indicate the overlap between the comparisons (the number of shown intersects in [E] was limited to 9). The bar plot on the right-hand side indicates the total number of altered proteins compared with HDs.

respective LiP-MS profiles. The proteotypes shared structurally perturbed proteins that enriched for 15 GO terms including cytoskeletal-, protein degradation-, and calcium-related pathways (GO keywords ''cytoskeleton'', ''actin-binding'', ''Ubl conjugation,'' and ''calcium'') and calcium-binding EF-hand proteins (Figures S1B and S1C). Importantly, however, glycoprotein abundance levels and structural integrity remained unchanged in context of heterozygous, but not homozygous, *CALR* mutations. In contrast, calcium- or cytoskeleton-related processes were similarly affected in both genotypes. We conclude that glycoprotein maturation is only negatively impacted in the homozygous state, whereas other CALR-mediated processes are less dependent on the mutational burden (Figure S1B).

Table 1. List of patient samples used in the study

PID	Group	Disease group	MF subtype	Age (years)	Sex
1	CALR type 1	MF	PET-MF	71	M
2	CALR type 1	MF	PMF	47	F
3	CALR type 1	MF	PMF	58	M
4	CALR type 1[a]	MF	PMF	50	F
5	CALR type 1	ET	–	53	M
6	CALR type 1	ET	–	63	F
7	CALR type 1	ET	–	69	M
8	CALR type 2	MF	PET-MF	89	M
9	CALR type 2[a]	MF	PET-MF	69	M
10	CALR type 2[a]	MF	PMF	81	M
11	CALR type 2	ET	–	43	F
12	CALR type 2	ET	–	76	F
13	CALR type 2	ET	–	61	M
14	CALR type 2	ET	–	45	M
15	JAK2	MF	PMF	64	F
16	JAK2	MF	PMF	86	M
17	JAK2	MF	PMF	53	M
18	JAK2	MF	PET-MF	79	F
19	JAK2	ET	–	55	M
20	JAK2	ET	–	65	F
21	JAK2	ET	–	65	M
22	JAK2	ET	–	60	M
23	HD	HD	–	54	M
24	HD	HD	–	64	F
25	HD	HD	–	60	M

PID, patient identification number; PMF, primary myelofibrosis; PET-MF, post essential thrombocythemia myelofibrosis; M, male; F, female. Related to Figure 1.
[a]Patient has a homozygous *CALR* mutation.

CALR mutations induce a localized conformational shift in calcium-regulated proteins, whereas glycoproteins exhibit global structural perturbations

To further delineate the impact of *CALR* mutations on glycoproteins and calcium-regulated proteins, we mapped the structurally altered peptides detected in homozygous *CALR*-mutated granulocytes to the protein sequence of representative members of each protein group (Figure 3A). Interestingly, we observed a high number of structurally altered peptides for the glycoprotein MPO, which spanned the entire sequence of the protein and were not limited to specific domains of the mature protein (Figure 3B). This suggests a global rearrangement of the protein, which could be caused by misfolding. Also, cathepsin S (CTSS), another abundant neutrophilic glycoprotein, displayed similar LiP patterns, while the other glycoproteins detected in the screen showed too little sequence coverage to perform a similar analysis (Figure 3C). We next assessed the site of structural rearrangements in calcium-regulated proteins by mapping the peptides. In contrast to glycoproteins, the conformational changes of calcium-regulated proteins predominantly occurred in functional calcium-binding domains such as EF-hands or EF-related hinge areas (as shown for the representative members LCP1 and S100A12), and EF-hand domains also enriched in the GO analysis (Figures 3D–3G). Among the non-glycosylated proteins, various upregulated cytoskeletal proteins also displayed a high degree of structural alterations, which may reflect altered cytoskeletal assembly dynamics in *CALR*-mutated MPNs (data not shown).

Homozygous *CALR* mutations phenocopy a CALR knockout with respect to glycoprotein folding

To further confirm that homozygous *CALR* mutations lead to CALR loss of function, we next investigated the CMK acute megakaryocytic leukemia cell line with a CALR knockout (KO) or a hemizygous *CALR* mutation by LiP-MS. CMK cells with a hemizygous *CALR* mutation contain a *CALR* allele with a premature stop codon and carry a *CALR* mutation on the remaining allele, therefore resembling a homozygous *CALR* mutation. We profiled the protein levels of 3,828 proteins and detected 22,124 structurally altered peptides mapping to 2,914 proteins (Figure 4A). We confirmed that the CALR protein levels of CMK cells with a hemizygous CALR mutation were similarly reduced when compared with patients with a homozygous *CALR* mutation (Figure 4B). Furthermore, the impact of hemi- or homozygous *CALR* mutations on the proteome were comparable to CALR KO (Figure 4B). The GO analysis revealed that signaling proteins, glycoproteins, and disulfide-bond-containing proteins were the only protein groups that exhibited significantly altered protein levels and structural changes across all three proteotypes (Figure 4C; Tables S2 and S3).

Next, we compared the proteome of CALR KO with CALR hemizygous CMK cells to investigate mechanisms that may affect glycoprotein integrity. The proteotypes of CMK CALR KO and CMK *CALR* hemizygous cells only shared approximately 20% of structurally altered or differentially expressed proteins (Figure 4D). This implies that hemizygous *CALR*-mutated CMKs only partially phenocopy CALR KO CMKs. However, the altered proteins shared between both genotypes significantly enriched for processes that were differentially regulated in patients with homozygous *CALR* mutations such as the calcium-regulated-, ubiquitination-, and protein-folding pathways (Table S4). Furthermore, we interpreted the abundance and structural changes detected in various chaperones, including the CALR-associated chaperones ERp57 (PDIA3) or CYPB (PPIB), as further indication of protein misfolding (Figure 4E). Taken together, our data suggest that hemi- and homozygous CALR mutations affect protein folding and glycoprotein integrity due to CALR loss of function.

Restoration of intracellular CALR mutant expression does not rescue MPO deficiency

Glycoproteins exhibited structural perturbations in patients with MPN with homozygous *CALR* mutations and our previous data

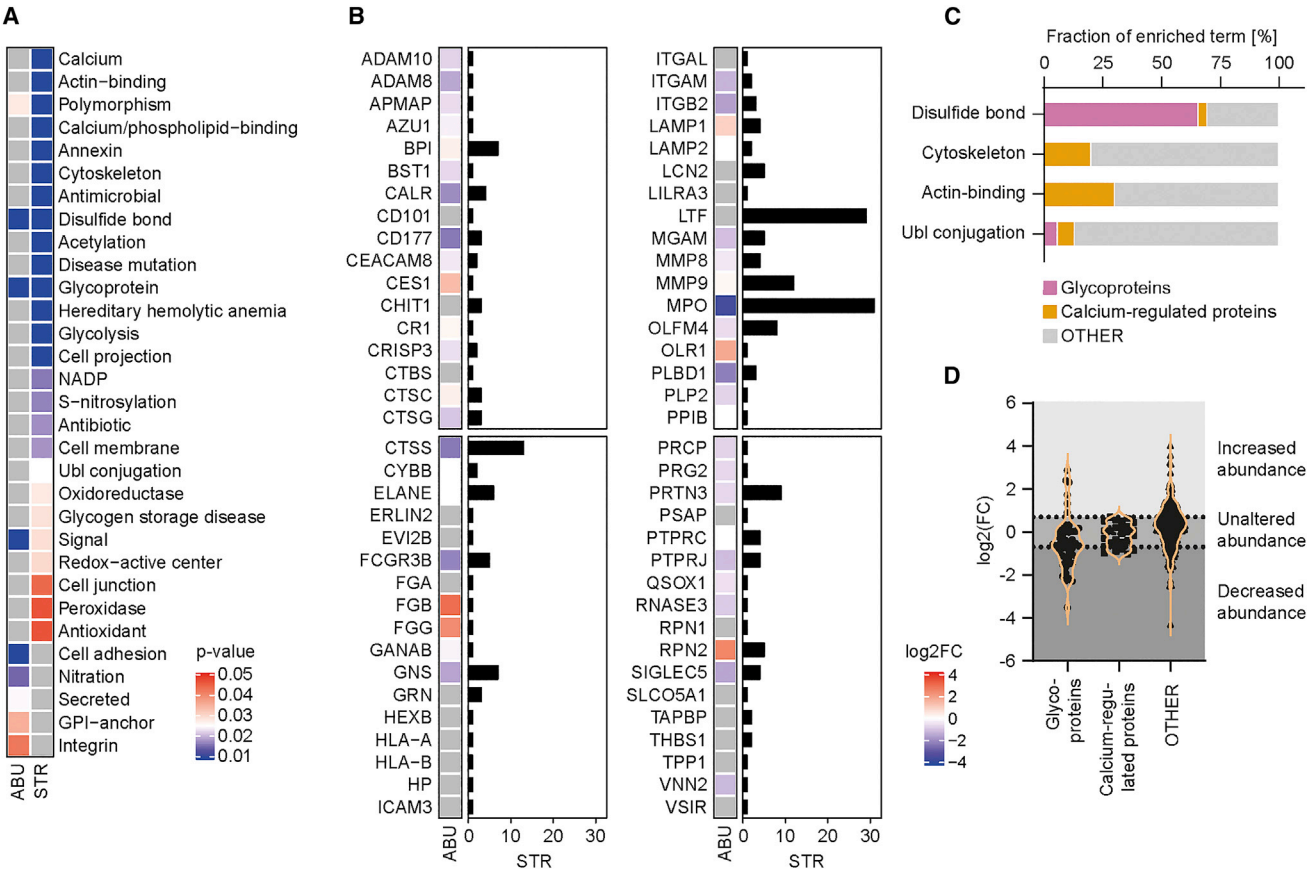

Figure 2. Gene ontology enrichment analysis reveals that homozygous *CALR* mutations perturb the glycoproteome and differentially affect protein subclasses

Proteomes of patients with homozygous *CALR* mutations were compared with *JAK2*-mutated MF controls.

(A) Gene ontology (GO) enrichment analysis of proteins with altered abundance levels and/or structurally altered peptides (DAVID Functional Annotation Bioinformatics Microarray Analysis GO enrichment tool). Heatmap shows significantly enriched UniProt keyword terms (adjusted [adj.] $p < 0.05$). Gray values represent missing values. ABU, enriched on the abundance level; STR, enriched on the structural level.

(B) Glycoproteins that indicated structural alterations. For each glycoprotein, the abundance levels (ABUs) and the amount of significantly structurally altered peptides (STRs) is indicated.

(C) Barplot showing fractions of glycoproteins, calcium-regulated proteins, or all remaining proteins (OTHER) proteins of respective GO terms "disulfide bond," "cytoskeleton," "actin-binding," and "Ubl conjugation."

(D) Abundance changes of proteins with structural alterations in homozygous *CALR*-mutated MF versus *JAK2*-mutated MF controls.

suggested a posttranslational defect in MPO biosynthesis.[23] However, the mechanism for this posttranslational maturation defect remains to be elucidated. Consequently, we next investigated whether an altered CALR chaperone function may account for disturbed proteostasis in the presence of *CALR* mutations. We selected MPO as a candidate protein to further elucidate the mechanisms that lead to structural proteome changes in the presence of *CALR* mutations. CALR associates with apopro MPO, which can be detected together with the reduced heavy chain (HC) of the mature MPO monomer (Figure 5A).[31,32] We first investigated whether increased secretion of CALR MUT resulted in a quantitative chaperone defect caused by low CALR chaperone availability within the ER. To test this assumption, we knocked out CALR expression in the promyeloblast HL-60 cell line using CRISPR-Cas9. Indeed, MPO protein expression was reduced in HL-60 CALR KO cells, which phenocopy primary granulocytes from patients with a homozygous *CALR* mutation (Figure 5B). To reliably detect the mutant CALR protein, we next used an antibody that specifically recognizes the mutant C terminus. CALR KO cells expressed low levels of apopro MPO precursors, which could not be rescued by overexpression of the CALR MUT variants T1 or T2 (Figure 5C). Moreover, restoring intracellular levels of CALR MUT by blocking its secretion with brefeldin A (BFA) did not restore apopro MPO levels. We further confirmed our findings in a second model that consisted of CALR KO K42 mouse embryonic fibroblasts co-transfected with human CALR and MPO (Figure 5D). In accordance with our previous finding, the MPO expression was equally low in K42 cells lacking CALR and their counterparts that expressed CALR MUT T1 or T2. In addition, we observed that the artificially induced secretion of CALR wild type (WT), which lacks the ER-retention signal, also leads to strongly

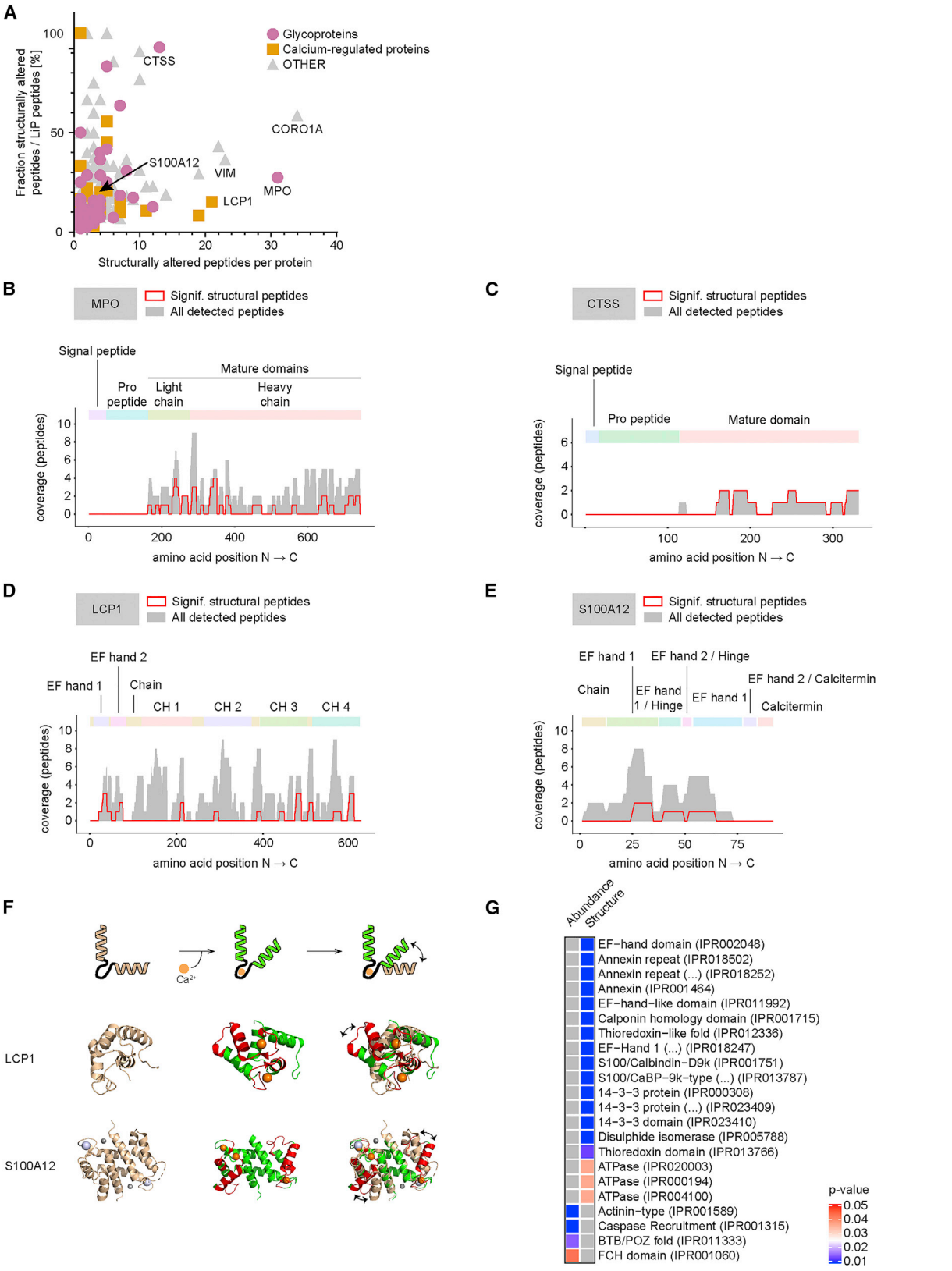

(legend on next page)

reduced MPO levels (Figures 5D and S2A). To rule out BFA-induced artifacts on MPO expression, we retained CALR MUT within the ER by reendowing CALR MUT T1 or T2 with the KDEL sequence, leading to a 9 (±0.6)-fold and 6 (±0.8)-fold increase of intracellular levels, respectively (Figure S2B). We backed our previous observation that retention of CALR MUT does not result in higher apopro MPO expression (Figure 5D). We, therefore, concluded that apopro MPO levels are equally low in the absence of CALR or the presence of CALR MUT. However, reduced intracellular levels of CALR MUT are not the sole mechanism causing MPO deficiency since the restoration of CALR MUT expression in the ER did not correct apopro MPO expression.

CALR mutants bind glycoproteins via the lectin holdase domain with reduced affinity but cannot bind to the foldase ERp57

We, therefore, investigated whether *CALR* mutations impact the chaperone function of CALR. More precisely, CALR functions as a lectin holdase that binds to the glycan residue of the glycoprotein precursor. Furthermore, CALR functions as an adaptor that brings foldases and glycoprotein precursors into close proximity, which supports the rearrangement of disulfide bonds or residues of the maturing glycoprotein.[15] When comparing homozygous *CALR*-mutated proteomes with *JAK2*-mutated controls, we did not detect any significant structural changes in the CALR C terminus. However, detecting structural changes in the mutant C terminus of CALR poses challenges. First, the frameshifted amino acid sequence may generate peptides that do not have a comparable counterpart in the WT samples. Second, the high occurrence of trypsin-cutting sites in the CALR C terminus impedes the sufficient generation of long-enough MS peptides (Figures S4A and S4B). We detected four CALR-specific structurally altered peptides in the N- and P-domains, suggesting structural alterations of mutant CALR and/or altered protein binding (Figure 6A). In accordance, one peptide mapped into the N-terminal lectin-binding site of an available murine CALR structure[34] (Figure 6B). We, therefore, assessed the holdase function of the CALR variants using a proximity ligation assay (PLA) and an ELISA-based binding assay to probe for binding between MPO and CALR (Figures 6C and 6D). Our data suggested that CALR MUT T1 and T2 bind to MPO, and we noted an increased number of CALR MUT T2-MPO complexes compared with their CALR MUT T1-MPO counterparts in the PLA (Figure 6C). The higher intracellular CALR MUT T2 levels may explain this difference (see Figures 5C and 5D). Blocking the secretion of the CALR mutants further increased the number of CALR MUT-MPO complexes. Our PLA setup did not allow us to directly compare MPO binding with CALR WT and with CALR MUT since CALR WT- and CALR MUT-specific antibodies were used for protein detection, respectively. Thus, to better quantify the amount of MPO bound to the CALR variants, we next overexpressed and purified glutathione-s-transferase (GST)-tagged CALR variants (Figures S3A and S3B). The immobilized GST-CALR constructs were then incubated with purified MPO (Figure 6D) or MPO-containing HL-60 lysates (Figure S3C). The binding between CALR and MPO was quantified using an anti-MPO antibody and a horseradish-peroxidase-mediated ELISA-based readout. In line with altered proteolytic patterns in the CALR MUT lectin-binding site, we observed a significant shift in the binding curves of GST-CALR MUT T1 and T2 to purified MPO compared with GST-CALR WT. This suggests that CALR MUT has a reduced MPO holdase activity compared with CALR WT. In conclusion, our data show that CALR MUT exhibits a mixed chaperone defect comprised of quantitative and qualitative attributes.

The LiP-MS screen indicated that the majority of structurally altered glycoproteins contained disulfide bridges. Therefore, we next assessed whether CALR MUT can still bind to foldases. Since the foldase ERp57 is involved in the maturation of MPO, we queried our LiP-MS dataset for patterns indicative of a potential defect of the CALR MUT-ERp57-MPO-complex assembly. Indeed, three out of the four CALR-specific structurally altered peptides mapped to the beginning of the P-domain of CALR MUT, suggesting an altered occupation of the P-domain by foldases (Figures 6A and 6B). There is no published crystal structure of the CALR-ERp57-MPO complex. Instead, we used the MHC peptide-loading complex (PLC) since, as for MPO, MHC class I requires both CALR and ERp57 for maturation.[35] Moreover, MHC class I is also a glycoprotein chaperoned by CALR and might be similarly affected as MPO since MHC class I expression is reduced in CALR MUT-expressing cell lines.[24] The structurally altered peptides mapped close to protein-protein interaction surfaces of the PLC members, suggesting that a suboptimal assembly of CALR to co-chaperones could be responsible for the generation of the structurally altered peptides (Figure 6E). We detected structurally altered peptides that map adjacent to the interaction surface of the CALR-associated foldase CYPB, which, similar to

Figure 3. *CALR* mutations induce a localized conformational shift in calcium-regulated proteins, whereas glycoproteins exhibit global structural perturbations

(A) Scatterplot visualizing the total number of structurally altered peptides per protein (x axis) versus the fraction of structurally altered peptides in all detected peptides for each protein (y axis). Proteins are grouped in three categories: glycoproteins, calcium-regulated/related proteins, and all other proteins. Representative members of each group used for subsequent structurally altered peptide mapping are shown.

(B–E) Panels showing the mapping of structurally altered peptides to the amino acid sequence of MPO, CTSS, LCP1, and S100A12. The red line indicates the structural change at each amino acid position of the protein polypeptide chain (expressed as coverage since multiple peptides can map to the same area). The gray area indicates the total amount of LiP peptides detected at each amino acid position.

(F) Representative members of EF-hand-containing proteins LCP1 and S100A12. Structurally altered peptides (red) were mapped to publicly available protein structures (green) of calcium-free (wheat-colored) or calcium-bound (green) structures of LCP1 (PDB: 5JOL and 5JOJ) and S100A12 (PDB: 2WC8 and 1E8A). Calcium ions are shown as orange spheres.

(G) GO enrichment as described in Figure 2A for structural motifs (INTERPRO) that significantly enriched in patients with MF with homozygous *CALR* mutations compared with *JAK2*-mutated MF controls.

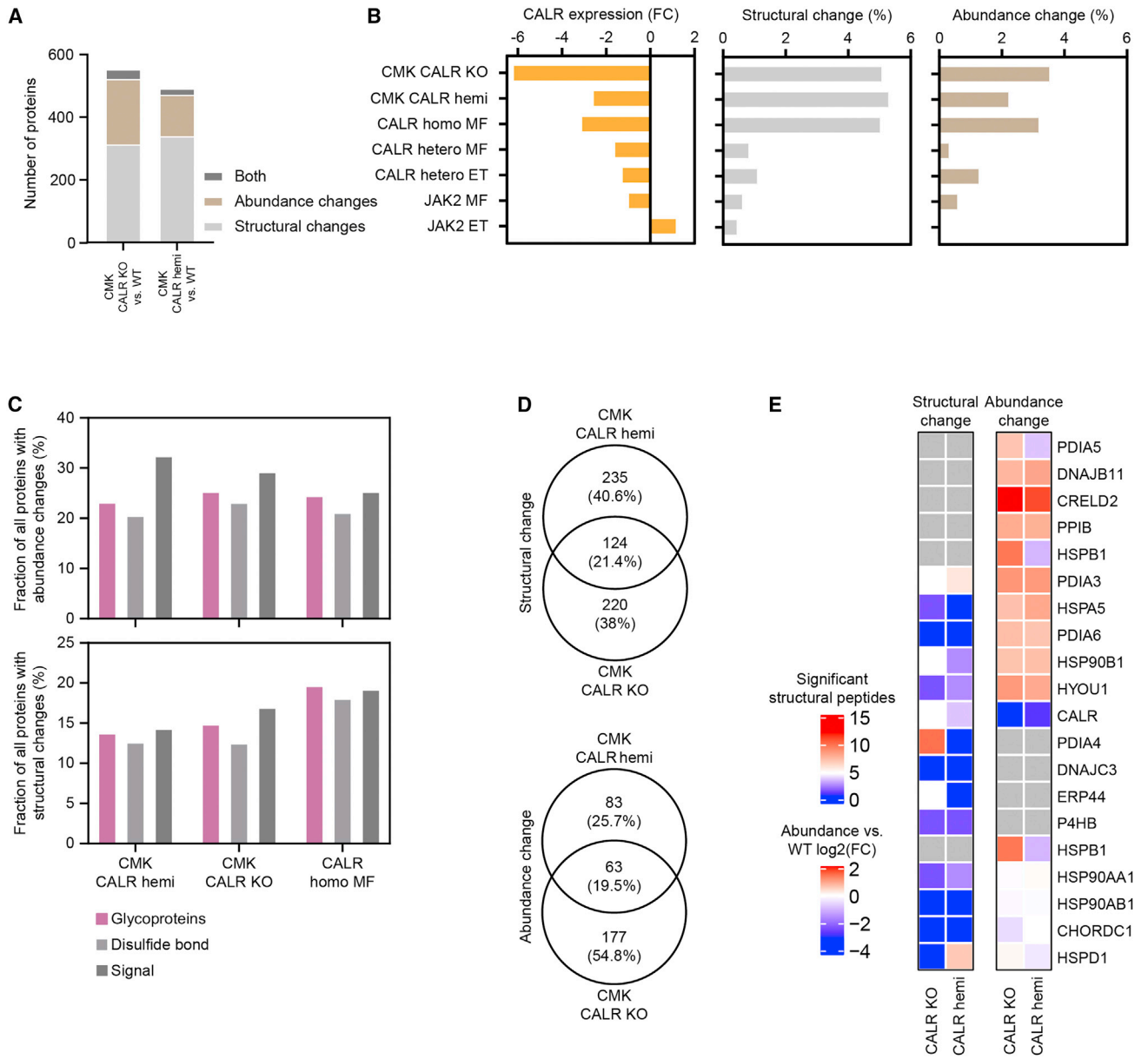

Figure 4. Homozygous *CALR* mutations phenocopy a CALR knockout with respect to glycoprotein folding

(A) Number of proteins with altered abundance and/or structural changes in CMK CALR knockout (KO) or CMK CALR hemizygous (hemi) cell lines compared with CMK WT controls.

(B) Number of proteins with altered abundance and/or structural changes for CMK CALR KO, CMK CALR hemi proteomes (versus CMK WT controls), or primary granulocyte proteomes (versus HD controls). For each proteotype, the fraction of proteins with altered structure or protein levels from the total amount of detected proteomes is indicated.

(C) UniProt keyword terms that significantly enriched on an abundance and structural level for CMK CALR KO (versus CMK WT), CMK CALR hemi (versus CMK WT), and CALR homozygous MF patient proteotypes (versus JAK2 MF controls). Bar plots express fraction of proteins of all proteins with abundance/structural changes that enriched for the respective GO term.

(D) Amount of proteins with altered structure or abundance that are shared between the CMK CALR KO or CALR hemi proteomes.

(E) Heatmap showing abundance levels and structural perturbations for selected chaperones of the significantly enriched GO terms "ER" and "chaperone" (see also Table S4).

ERp57, also binds the CALR P-domain (Figure S5).[36] This is an additional indication for a reduced recruitment of foldases to the CALR MUT P-domain. The PLA assay confirmed the *in situ* LiP-MS data since CALR WT, but not CALR MUT, bound ERp57 (Figure 6F). In summary, we conclude that the mutant C terminus partially affects the binding of CALR MUT to glycoproteins, which does not fully explain the mechanism of glycoprotein deficiency. Another contributing factor is the lack of

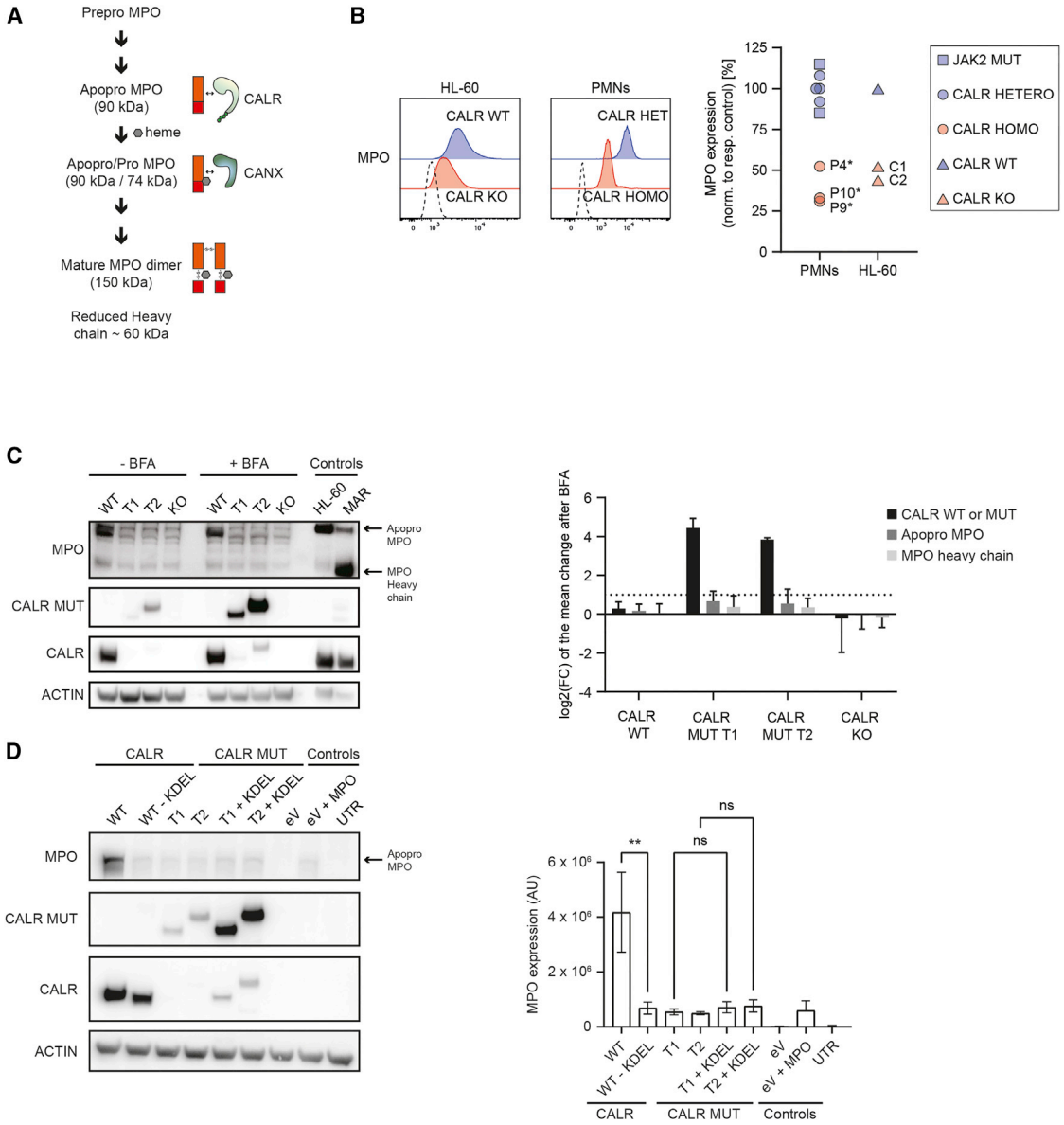

Figure 5. Restoration of intracellular CALR mutant expression does not rescue MPO deficiency

(A) Cartoon depicting the maturational stages of MPO and its interaction with CALR and calnexin (CANX).[31–33]

(B) Left, representative flow cytometry histograms showing MPO expression in HL-60 CALR KO clone 1 cells (red) compared with PMNs of patient 9 with a homozygous *CALR* mutation (P9, red). The respective WT CALR controls and unstained samples are indicated (blue and dashed line, respectively). Right, MPO expression of primary PMNs of patients with homozygous *CALR* mutations in the cohort (patients 4, 9, and 10) compared with *JAK2*-mutated, heterozygous *CALR*-mutated controls, HL-60 CALR KO clones 1 (C1) and 2 (C2), and parental HL-60 (CALR WT).

(C) Left, CALR (WT) or CALR MUT (T1 or T2) were transduced into CALR KO HL-60 clone 1 cells (KO), and secretion was blocked using brefeldin A (BFA). MARIMO (MAR) cells are used as an additional positive control to confirm the correct location of apopro MPO and MPO heavy-chain bands in western blots. Representative experiment shown (n = 2). Right, quantification of CALR and MPO log2(FC) expression change before and after BFA treatment (mean ± SD, n = 2).

(D) Left, the CALR KO murine fibroblast cell line K42 was co-transfected with MPO and either CALR (WT), CALR MUT T1 or T2, or "secretion-resistant" CALR MUT T1 or T2 mutants expressing KDEL sequences (+KDEL). eV, empty vector; eV + MPO, empty vector with MPO; UTR, untransfected control cells. A representative experiment is shown (n = 2). Right, quantification of MPO expression (mean ± SD, n = 2; see also Figure S2). ns, not significant; asterisks indicate p values as calculated by ordinary one-way ANOVA: *p ≤ 0.05; **p ≤ 0.01; ***p ≤ 0.001; ****p ≤ 0.0001.

association observed between ERp57 and CALR MUT, which may impede the ERp57-mediated rearrangement of disulfide bonds within the nascent MPO chain, leading to a conformational arrest at the apopro MPO level.

Overall, we infer that *CALR* mutations lead to a complex combination of quantitative and qualitative loss-of-function traits, which compromise CALR MUT chaperone function. The LiP-MS data show that this mixed chaperone defect affects the

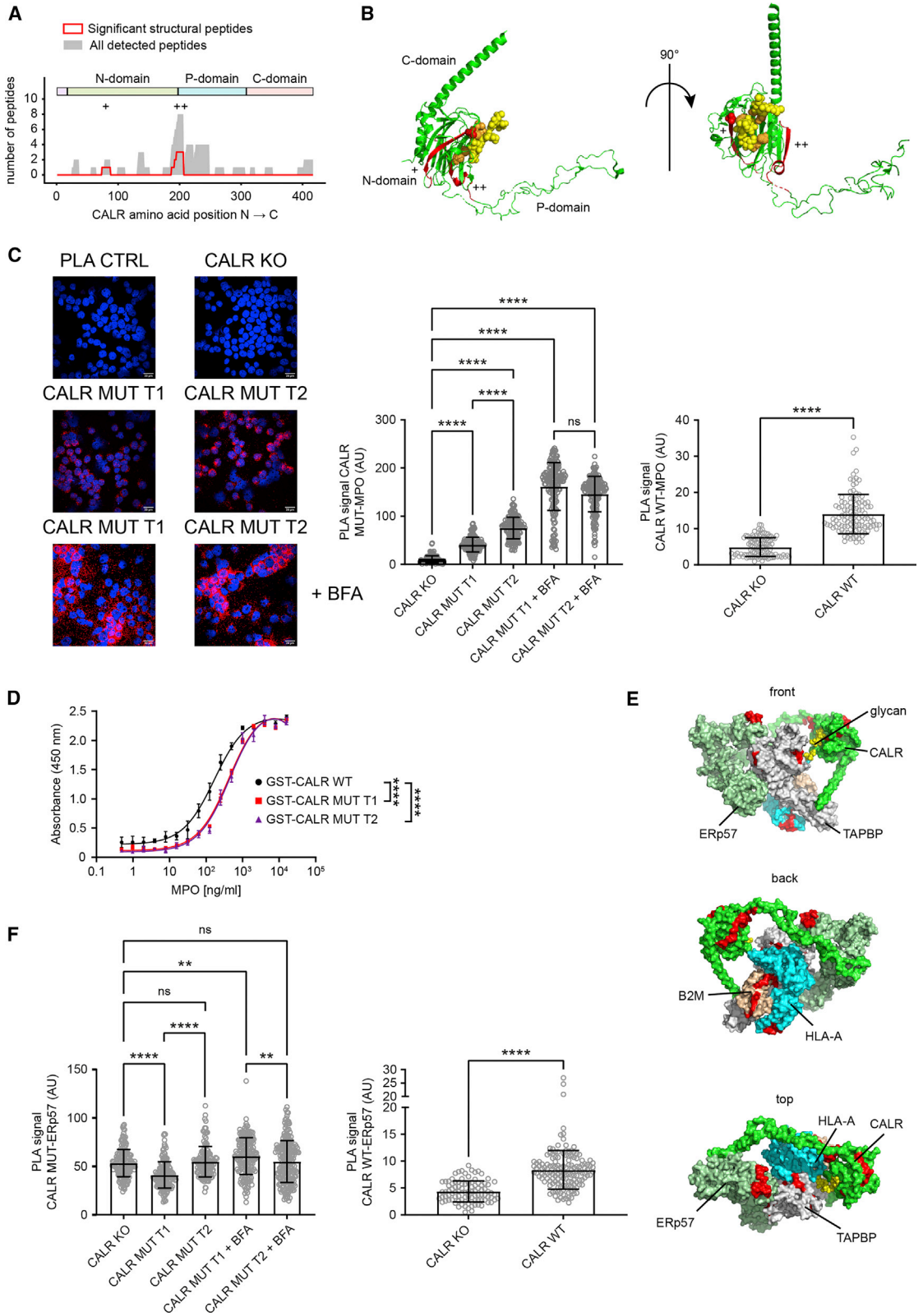

(legend on next page)

structural integrity of the glycoproteome of patients with homozygous *CALR* mutations.

DISCUSSION

By combining the *in situ* approach of LiP-MS with mechanistic data, we demonstrate that a complex amalgam of quantitative and qualitative chaperone defects of CALR MUT compromises glycoprotein maturation. Patients with hetero- and homozygous *CALR* mutations exhibited structural perturbations of cytoskeletal and calcium-related proteins, but the protein expression levels remained unaffected. In contrast, homozygous *CALR* mutations affected both protein expression and structural integrity of glycoproteins. The LiP-MS data imply that this is the consequence of CALR MUT loss-of-function attributes since chaperones, ubiquitin-dependent protein degradation pathways, and glycoprotein integrity were equally affected in patient granulocytes with homozygous *CALR* mutations and CALR KO CMK cells. The increased detection of structurally altered peptides within the N-terminal lectin domain of CALR MUT suggests that an altered occupation of the lectin-binding site could expose it to increased LiP protease digestion. We confirmed this by demonstrating a decreased affinity of the lectin domain to the soluble CALR client MPO. Our immunological protein-protein binding assays involve fusion proteins and/or rely on antibody specificity, thereby allowing a cautious interpretation of reported protein interactions. However, the data do support recent findings showing that *CALR* mutations affect the glycoprotein binding of CALR MUT in a client-specific fashion to membrane-bound CALR clients TPOR and MHC class I.[18,24] Experiments with truncated CALR MUT variants suggested that the mutant C terminus affects the N-terminal lectin binding to the TPOR indirectly via the P-domain.[3] Possibly, glycoprotein binding by CALR MUT is further influenced by collaborating chaperones that bind the P-domain. In addition to affecting the holdase function, the mutant C terminus also prevented the foldase ERp57 from binding the CALR P-domain, which is consistent with previous data.[19,37] The altered structural fingerprints in CALR, ERp57, and CYPB imply that this binding defect could extend to other CALR-associated foldases.[34,38] We conclude that the disulfide bridges of glycoprotein precursors cannot be correctly rearranged in the presence of CALR MUT, which consequently causes a conformational arrest. Future studies unraveling the crystal structures of CALR MUT will shed more light on the impact of the mutant C terminus on the holdase and the co-chaperone-mediated foldase function of the CALR chaperone complex.

By characterizing the LiP profiles of primary neutrophils, we demonstrate the applicability of LiP-MS to patient-derived cell populations. One limitation of LiP-MS is the need of high protein concentrations since the proteins have to be extracted under native conditions. More precisely, our studies show that >10 million neutrophils are needed for LiP-MS, which at this point precludes us from analyzing rare cell populations such as hematopoietic stem and progenitor cells and megakaryocytes.

Recently, upregulation of ER chaperones as part of the UPR was described in primary $CD34^+$ cells from patients with MPN with *CALR* mutations.[21] Our proteotype profiling shows that the conformational integrity of glycoproteins is mainly affected in the proteome of patients with homozygous *CALR* T1 and T2 mutations. This finding was particularly apparent in glycoproteins with a high peptide coverage such as MPO or CTSS, which both exhibited global structural alterations and a concomitant downregulation of protein abundance. Presumably, the UPR-induced upregulation of the remaining WT CALR copy in cells with heterozygous *CALR* mutations prevents reduced glycoprotein expression. In accordance with this notion, we did not observe reduced MPO in the context of heterozygous *CALR* mutations. Our data further imply that UPR chaperones cannot compensate for a complete loss of WT CALR, as observed in homozygous patients.[23] It remains to be determined whether increased protein degradation contributes to disease progression as described in patients with a high *CALR* mutant allele burden.[29,30] A link between differential activation of the UPR branches and the maintenance of healthy and leukemic stem cells has previously been established.[39,40] Moreover, CALR haploinsufficiency in a *CALR*-mutated mouse model augmented hematopoietic stem cell activity in a JAK-STAT-signaling-independent manner, which was paramount for MPN onset.[41] Since the UPR pathways rely on protein degradation pathways, it will be of interest to elucidate whether the targeting of protein degradation pathways may be strategically combined with existing treatment modalities for *CALR*-mutated MPNs.

Figure 6. CALR mutants bind glycoproteins via the lectin holdase domain with reduced affinity but cannot bind to the foldase ERp57

(A) The occurrence of structural changes across the CALR amino acid sequence (CALR WT versus mutant CALR variants). Significantly structurally altered peptides (red) and all detected peptides (shaded gray area) were mapped across the CALR protein sequence. The two protein segments with significantly altered peptides shown in the panel are also indicated in the protein structure (shown in B), as denoted by the +/++. Note that the peptide generation/coverage is low for the WT and mutant CALR C terminus due to differential protein sequences and the high occurrence of trypsin-cutting sites (Figures S4A and S4B).

(B) Structurally altered peptides (red) mapped to the protein structure (green) of murine CALR (PDB: 3RG0).[34] Orange spheres indicate residues (Phe74, Cys105, Met131, Cys137, His145, Ile147, Trp319) involved in the binding of the N-linked glycan of glycoproteins (yellow).

(C) Left panel, representative images of PLA probing the interaction of CALR and MPO (scale bar: 20 μm). PLA was performed using anti-MPO, anti-CALR, or anti-CALR MUT antibodies in CALR KO cells transduced with either CALR or CALR MUT T1 or T2. Secretion was blocked using BFA. In the PLA control, the primary CALR antibodies were omitted. Middle panel, PLA signal probing the interaction between MPO and CALR MUT (counted cells: KO = 112, T1 = 134, T2 = 157, T1 + BFA = 173, T2 + BFA = 175). Right panel, PLA signal of MPO and CALR WT (counted cells: KO = 113, WT = 111). Each bar plot shows pooled data (mean ± SD) from two independent experiments. Asterisks indicate p values as calculated by Kruskal-Wallis or Mann-Whitney test.

(D) Representative binding curves of immobilized purified GST-CALR variants to MPO (one of two independent experiments shown). Asterisks indicate p values as calculated by an ordinary one-way ANOVA.

(E) Structurally altered peptides (red) mapped to the peptide loading complex members CALR, B2M, ERp57, HLA-A, and TAPBP (PDB: 6ENY).

(F) CALR-ERp57 interaction probed by PLA as described above. Left panel, PLA signal of ERp57 and CALR MUT (counted cells: KO = 178, T1 = 168, T2 = 135, T1 + BFA = 175, T2 + BFA = 216). Right panel, PLA signal of ERp57 and CALR (counted cells right: KO = 95, WT = 146).

p values as indicated in (C), (D), and (F): ns, not significant; *$p \leq 0.05$; **$p \leq 0.01$; ***$p \leq 0.001$; ****$p \leq 0.0001$.

In contrast to glycoprotein folding, other pathways such as calcium-related and cytoskeletal processes (among others) were affected in both hetero- and homozygous CALR-mutated cells. For instance, calcium-regulated proteins were mainly affected on a structural level in homozygous *CALR*-mutated proteomes. Our list of calcium-regulated proteins included several members of the S100 family that adjust their biological activity to calcium levels using EF-hand domains. The significantly enriched conformational rearrangements within calcium-regulated domains were likely caused by aberrant calcium homeostasis, as previously reported in *CALR*-mutated cells.[6,19] Presumably, altered activation of S100 proteins may also contribute to the clinical differences observed between patients with *CALR*- and *JAK2*-mutated MPN.[6,42]

In conclusion, we show that *CALR* mutations compromise CALR chaperone function with profound implications on glycoproteins and other protein classes in patients with homozygous *CALR* mutations. This study contributes to a better understanding of JAK-STAT-signaling-independent mechanisms in patients with MPN with *CALR* mutations, which might improve future patient stratification and treatment regimens. Finally, our results encourage the application of LiP-MS to primary samples of patients with hematopoietic stem cell neoplasms and other diseases characterized by protein misfolding.

A list of abbreviations can be found in Table S5.

Limitations of the study

We conducted our LiP-MS analysis in primary neutrophils and acute megakaryocytic leukemia cell lines, focusing on glycoproteins, but our findings encourage extending the investigation to other protein groups and more rare cell types essential for MPN biology including hematopoietic stem cells and megakaryocytes. This will be possible once LiP-MS allows the analysis of smaller cell numbers.

We are aware that the *in vitro* characterization of the MPO deficiency only partly validates the assumption that glycoprotein misfolding is responsible for most *in situ* structural perturbation of the glycoproteome since we did not evaluate the interaction of the mutant CALR glycoprotein chaperone to other glycoprotein clients. Our protein-protein interaction data obtained by immunological assays provide valuable insights on altered mutant CALR protein biology. However, despite using validated antibodies and the appropriate controls, we cannot fully rule out any effects of antibody specificity or protein tags on *in vitro* protein binding. This study did not dissect the mutant CALR interactome further by employing more robust surface plasmon resonance assays. Also, the generation of crystal structures for human WT and mutant CALR would be of immense experimental value to further investigate pathological protein interactions with CALR mutants.

Lastly, our HL-60 and K42 cell line models are highly valuable but remain inferior to primary cells since they exhibit a CALR KO or express the CALR variants at non-physiological levels.

STAR★METHODS

Detailed methods are provided in the online version of this paper and include the following:

- KEY RESOURCES TABLE
- RESOURCE AVAILABILITY
  - Lead contact
  - Materials availability
  - Data and code availability
- EXPERIMENTAL MODEL AND SUBJECT DETAILS
  - Primary mass spectrometry samples
  - Cell lines
  - Generation of *CALR* knockout HL-60 cells
- METHOD DETAILS
  - DNA plasmids and lentiviral transduction
  - Western blot
  - Proximity ligation assay (PLA)
  - Flow cytometry
  - Elisa-based binding assay
  - Limited proteolysis coupled to mass spectrometry (LiP-MS)
- QUANTIFICATION AND STATISTICAL ANALYSIS

SUPPLEMENTAL INFORMATION

Supplemental information can be found online at https://doi.org/10.1016/j.celrep.2022.111689.

ACKNOWLEDGMENTS

We thank Asuka Fry and Patrizia Belleda for processing patient samples. A.P.A.T. is supported by the Professor Dr. Max Cloetta Foundation and the Swiss National Science Foundation (SNF project grant 310030_170237). B.W. acknowledges support from ETH Zurich, D-HEST (BMPP), a Swiss National Science Foundation grant (grant 31003A_160259), and the Personalized Health and Related Technologies (PHRT) strategic focus area of ETH. A.P.A.T. and P.M.S. are recipients of a Hematology Research grant by the Jacques & Gloria Gossweiler Foundation in cooperation with the Swiss Society of Hematology.

AUTHOR CONTRIBUTIONS

P.M.S. designed and performed research, analyzed data, and wrote the manuscript; L.M., M.H., M.L., M.C.H., and M.H.E.W. performed research and analyzed data; C.A.M. analyzed data; V.L. and A.K.K.L. performed research; B.W. and P.P. provided strategic support, designed research, and revised the manuscript; A.P.A.T. designed research, directed the studies, analyzed data, and wrote the manuscript; all authors reviewed the manuscript.

DECLARATION OF INTERESTS

The authors declare no competing interests.

Received: July 8, 2021
Revised: July 17, 2022
Accepted: October 27, 2022
Published: November 22, 2022

REFERENCES

1. Deutsch, E.W., Bandeira, N., Sharma, V., Perez-Riverol, Y., Carver, J.J., Kundu, D.J., García-Seisdedos, D., Jarnuczak, A.F., Hewapathirana, S., Pullman, B.S., et al. (2020). The ProteomeXchange consortium in 2020: enabling 'big data'approaches in proteomics. Nucleic Acids Res. *48*, D1145–D1152.
2. Tefferi, A., and Pardanani, A. (2015). Myeloproliferative neoplasms: a contemporary review. JAMA Oncol. *1*, 97–105.

3. Araki, M., Yang, Y., Masubuchi, N., Hironaka, Y., Takei, H., Morishita, S., Mizukami, Y., Kan, S., Shirane, S., Edahiro, Y., et al. (2016). Activation of the thrombopoietin receptor by mutant calreticulin in CALR-mutant myeloproliferative neoplasms. Blood *127*, 1307–1316.
4. Nangalia, J., Massie, C.E., Baxter, E.J., Nice, F.L., Gundem, G., Wedge, D.C., Avezov, E., Li, J., Kollmann, K., Kent, D.G., et al. (2013). Somatic CALR mutations in myeloproliferative neoplasms with nonmutated JAK2. N. Engl. J. Med. *369*, 2391–2405.
5. Klampfl, T., Gisslinger, H., Harutyunyan, A.S., Nivarthi, H., Rumi, E., Milosevic, J.D., Them, N.C.C., Berg, T., Gisslinger, B., Pietra, D., et al. (2013). Somatic mutations of calreticulin in myeloproliferative neoplasms. N. Engl. J. Med. *369*, 2379–2390.
6. Pietra, D., Rumi, E., Ferretti, V.V., Di Buduo, C.A., Milanesi, C., Cavalloni, C., Sant'Antonio, E., Abbonante, V., Moccia, F., Casetti, I.C., et al. (2016). Differential clinical effects of different mutation subtypes in CALR-mutant myeloproliferative neoplasms. Leukemia *30*, 431–438.
7. Michalak, M., Robert Parker, J.M., and Opas, M. (2002). Ca2+ signaling and calcium binding chaperones of the endoplasmic reticulum. Cell Calcium *32*, 269–278.
8. Nakamura, K., Zuppini, A., Arnaudeau, S., Lynch, J., Ahsan, I., Krause, R., Papp, S., De Smedt, H., Parys, J.B., Muller-Esterl, W., et al. (2001). Functional specialization of calreticulin domains. J. Cell Biol. *154*, 961–972.
9. Michalak, M., Groenendyk, J., Szabo, E., Gold, L.I., and Opas, M. (2009). Calreticulin, a multi-process calcium-buffering chaperone of the endoplasmic reticulum. Biochem. J. *417*, 651–666.
10. Hebert, D.N., Foellmer, B., and Helenius, A. (1996). Calnexin and calreticulin promote folding, delay oligomerization and suppress degradation of influenza hemagglutinin in microsomes. EMBO J. *15*, 2961–2968.
11. Hebert, D.N., and Molinari, M. (2007). In and out of the ER: protein folding, quality control, degradation, and related human diseases. Physiol. Rev. *87*, 1377–1408.
12. Saito, Y., Ihara, Y., Leach, M.R., Cohen-Doyle, M.F., and Williams, D.B. (1999). Calreticulin functions in vitro as a molecular chaperone for both glycosylated and non-glycosylated proteins. EMBO J. *18*, 6718–6729.
13. Leach, M.R., Cohen-Doyle, M.F., Thomas, D.Y., and Williams, D.B. (2002). Localization of the lectin, ERp57 binding, and polypeptide binding sites of calnexin and calreticulin. J. Biol. Chem. *277*, 29686–29697.
14. Leach, M.R., and Williams, D.B. (2003). Calnexin and Calreticulin, Molecular Chaperones of the Endoplasmic Reticulum (Calreticulin), pp. 49–62.
15. Kozlov, G., Muñoz-Escobar, J., Castro, K., and Gehring, K. (2017). Mapping the ER interactome: the P domains of calnexin and calreticulin as plurivalent adapters for foldases and chaperones. Structure *25*, 1415–1422.e3.
16. Elf, S., Abdelfattah, N.S., Chen, E., Perales-Patón, J., Rosen, E.A., Ko, A., Peisker, F., Florescu, N., Giannini, S., Wolach, O., et al. (2016). Mutant calreticulin requires both its mutant C-terminus and the thrombopoietin receptor for oncogenic transformation. Cancer Discov. *6*, 368–381.
17. Chachoua, I., Pecquet, C., El-Khoury, M., Nivarthi, H., Albu, R.-I., Marty, C., Gryshkova, V., Defour, J.-P., Vertenoeil, G., and Ngo, A. (2015). Thrombopoietin receptor activation by myeloproliferative neoplasm associated calreticulin mutants. Blood *127*, 1325–1335. blood-2015-2011-681932.
18. Araki, M., and Komatsu, N. (2017). Novel molecular mechanism of cellular transformation by a mutant molecular chaperone in myeloproliferative neoplasms. Cancer Sci. *108*, 1907–1912.
19. Di Buduo, C.A., Abbonante, V., Marty, C., Moccia, F., Rumi, E., Pietra, D., Soprano, P.M., Lim, D., Cattaneo, D., Iurlo, A., et al. (2020). Defective interaction of mutant calreticulin and SOCE in megakaryocytes from patients with myeloproliferative neoplasms. Blood *135*, 133–144.
20. Han, L., Schubert, C., Köhler, J., Schemionek, M., Isfort, S., Brümmendorf, T.H., Koschmieder, S., and Chatain, N. (2016). Calreticulin-mutant proteins induce megakaryocytic signaling to transform hematopoietic cells and undergo accelerated degradation and Golgi-mediated secretion. J. Hematol. Oncol. *9*, 45.
21. Nam, A.S., Kim, K.-T., Chaligne, R., Izzo, F., Ang, C., Taylor, J., Myers, R.M., Abu-Zeinah, G., Brand, R., Omans, N.D., et al. (2019). Somatic mutations and cell identity linked by Genotyping of Transcriptomes. Nature *571*, 355–360.
22. Salati, S., Genovese, E., Carretta, C., Zini, R., Bartalucci, N., Prudente, Z., et al. (2019). Calreticulin Ins5 and Del52 mutations impair unfolded protein and oxidative stress responses in K562 cells expressing CALR mutants. Sci. Rep. *9*, 1–14.
23. Theocharides, A.P.A., Lundberg, P., Lakkaraju, A.K.K., Lysenko, V., Myburgh, R., Aguzzi, A., Skoda, R.C., and Manz, M.G. (2016). Homozygous calreticulin mutations in patients with myelofibrosis lead to acquired myeloperoxidase deficiency. Blood *127*, 3253–3259.
24. Arshad, N., and Cresswell, P. (2018). Tumor-associated calreticulin variants functionally compromise the peptide loading complex and impair its recruitment of MHC-I. J. Biol. Chem. *293*, 9555–9569.
25. Feng, Y., De Franceschi, G., Kahraman, A., Soste, M., Melnik, A., Boersema, P.J., De Laureto, P.P., Nikolaev, Y., Oliveira, A.P., and Picotti, P. (2014). Global analysis of protein structural changes in complex proteomes. Nat. Biotechnol. *32*, 1036–1044.
26. Schopper, S., Kahraman, A., Leuenberger, P., Feng, Y., Piazza, I., Müller, O., Boersema, P.J., and Picotti, P. (2017). Measuring protein structural changes on a proteome-wide scale using limited proteolysis-coupled mass spectrometry. Nat. Protoc. *12*, 2391–2410.
27. Feng, Y., Beaton, N., Bruderer, R., Piazza, I., Picotti, P., and Reiter, L. (2020). LiP-Quant, an automated chemoproteomic approach to identify drug targets in complex proteomes. Cancer Res. *80*, 6404.
28. Leuenberger, P., Ganscha, S., Kahraman, A., Cappelletti, V., Boersema, P.J., von Mering, C., Claassen, M., and Picotti, P. (2017). Cell-wide analysis of protein thermal unfolding reveals determinants of thermostability. Science *355*, eaai7825.
29. Stengel, A., Jeromin, S., Haferlach, T., Meggendorfer, M., Kern, W., and Haferlach, C. (2019). Detection and characterization of homozygosity of mutated CALR by copy neutral loss of heterozygosity in myeloproliferative neoplasms among cases with high CALR mutation loads or with progressive disease. Haematologica *104*, e187–e190.
30. Cottin, L., Riou, J., Orvain, C., Ianotto, J.C., Boyer, F., Renard, M., Truchan-Graczyk, M., Murati, A., Jouanneau-Courville, R., Allangba, O., et al. (2020). Sequential mutational evaluation of CALR-mutated myeloproliferative neoplasms with thrombocytosis reveals an association between CALR allele burden evolution and disease progression. Br. J. Haematol. *188*, 935–944.
31. Hansson, M., Olsson, I., and Nauseef, W.M. (2006). Biosynthesis, processing, and sorting of human myeloperoxidase. Arch. Biochem. Biophys. *445*, 214–224.
32. Nauseef, W.M., McCormick, S.J., and Goedken, M. (1998). Coordinated participation of calreticulin and calnexin in the biosynthesis of myeloperoxidase. J. Biol. Chem. *273*, 7107–7111.
33. Nauseef, W.M. (2018). Biosynthesis of human myeloperoxidase. Arch. Biochem. Biophys. *642*, 1–9.
34. Kozlov, G., Pocanschi, C.L., Rosenauer, A., Bastos-Aristizabal, S., Gorelik, A., Williams, D.B., and Gehring, K. (2010). Structural basis of carbohydrate recognition by calreticulin. J. Biol. Chem. *285*, 38612–38620.
35. Blees, A., Januliene, D., Hofmann, T., Koller, N., Schmidt, C., Trowitzsch, S., Moeller, A., and Tampé, R. (2017). Structure of the human MHC-I peptide-loading complex. Nature *551*, 525–528.
36. Kozlov, G., Bastos-Aristizabal, S., Määttänen, P., Rosenauer, A., Zheng, F., Killikelly, A., Trempe, J.-F., Thomas, D.Y., and Gehring, K. (2010). Structural basis of cyclophilin B binding by the calnexin/calreticulin P-domain. J. Biol. Chem. *285*, 35551–35557.
37. Elf, S., Abdelfattah, N.S., Baral, A.J., Beeson, D., Rivera, J.F., Ko, A., Florescu, N., Birrane, G., Chen, E., and Mullally, A. (2017). Defining the requirements for the pathogenic interaction between mutant calreticulin and MPL in MPN. Blood *131*, 782–786.

38. Kozlov, G., and Gehring, K. (2020). Calnexin cycle–structural features of the ER chaperone system. FEBS J. *287*, 4322–4340.

39. van Galen, P., Kreso, A., Mbong, N., Kent, D.G., Fitzmaurice, T., Chambers, J.E., Xie, S., Laurenti, E., Hermans, K., Eppert, K., et al. (2014). The unfolded protein response governs integrity of the haematopoietic stem-cell pool during stress. Nature *510*, 268–272.

40. van Galen, P., Mbong, N., Kreso, A., Schoof, E.M., Wagenblast, E., Ng, S.W.K., Krivdova, G., Jin, L., Nakauchi, H., and Dick, J.E. (2018). Integrated stress response activity marks stem cells in normal hematopoiesis and leukemia. Cell Rep. *25*, 1109–1117.e5.

41. Shide, K., Kameda, T., Kamiunten, A., Ozono, Y., Tahira, Y., Yokomizo-Nakano, T., Kubota, S., Ono, M., Ikeda, K., and Sekine, M. (2020). Calreticulin haploinsufficiency augments stem cell activity and is required for onset of myeloproliferative neoplasms. Blood *136*, 106–118.

42. Tefferi, A., Lasho, T.L., Finke, C., Belachew, A.A., Wassie, E.A., Ketterling, R.P., Hanson, C.A., and Pardanani, A. (2014). Type 1 vs type 2 calreticulin mutations in primary myelofibrosis: differences in phenotype and prognostic impact. Leukemia *28*, 1568–1570.

43. Shide, K., Kameda, T., Yamaji, T., Sekine, M., Inada, N., Kamiunten, A., Akizuki, K., Nakamura, K., Hidaka, T., and Kubuki, Y. (2016). Calreticulin mutant mice develop essential thrombocythemia that is ameliorated by the JAK inhibitor ruxolitinib. Leukemia *31*, 1136–1144.

44. Gundry, M.C., Brunetti, L., Lin, A., Mayle, A.E., Kitano, A., Wagner, D., Hsu, J.I., Hoegenauer, K.A., Rooney, C.M., Goodell, M.A., and Nakada, D. (2016). Highly efficient genome editing of murine and human hematopoietic progenitor cells by CRISPR/Cas9. Cell Rep. *17*, 1453–1461.

45. Mughal, F.P., Bergmann, A.C., Huynh, H.U.B., Jørgensen, S.H., Mansha, I., Kesmez, M., Schürch, P.M., Theocharides, A.P.A., Hansen, P.R., Friis, T., et al. (2022). Production and characterization of peptide antibodies to the C-terminal of frameshifted calreticulin associated with myeloproliferative diseases. Int. J. Mol. Sci. *23*, 6803.

46. Schindelin, J., Arganda-Carreras, I., Frise, E., Kaynig, V., Longair, M., Pietzsch, T., Preibisch, S., Rueden, C., Saalfeld, S., Schmid, B., et al. (2012). Fiji: an open-source platform for biological-image analysis. Nat. Methods *9*, 676–682.

47. Rueden, C.T., Schindelin, J., Hiner, M.C., DeZonia, B.E., Walter, A.E., Arena, E.T., et al. (2017). ImageJ2: ImageJ for the next generation of scientific image data. BMC Bioinf. *18*, 1–26.

48. Malinovska, L., Cappelletti, V., Kohler, D., Piazza, I., Tsai, T.-H., Pepelnjak, M., et al. (2022). Proteome-wide structural changes measured with limited proteolysis-mass spectrometry: an advanced protocol for high-throughput applications. Nat. Protoc. *10*, 1038.

49. Cappelletti, V., Hauser, T., Piazza, I., Pepelnjak, M., Malinovska, L., Fuhrer, T., Li, Y., Dörig, C., Boersema, P., Gillet, L., et al. (2021). Dynamic 3D proteomes reveal protein functional alterations at high resolution in situ. Cell *184*, 545–559.e22.

50. Benjamini, Y., and Hochberg, Y. (1995). Controlling the false discovery rate: a practical and powerful approach to multiple testing. J. R. Stat. Soc. B Methodol. *57*, 289–300.

51. R Core Team (2013). R: A Language and Environment for Statistical Computing.

52. Conway, J.R., Lex, A., and Gehlenborg, N. (2017). UpSetR: an R package for the visualization of intersecting sets and their properties. Bioinformatics *33*, 2938–2940.

53. Gu, Z., Eils, R., and Schlesner, M. (2016). Complex heatmaps reveal patterns and correlations in multidimensional genomic data. Bioinformatics *32*, 2847–2849.

54. Wickham, H. (2016). ggplot2: Elegant Graphics for Data Analysis (Springer).

55. Huang, D.W., Sherman, B.T., and Lempicki, R.A. (2009). Systematic and integrative analysis of large gene lists using DAVID bioinformatics resources. Nat. Protoc. *4*, 44–57.

STAR★METHODS

KEY RESOURCES TABLE

REAGENT or RESOURCE	SOURCE	IDENTIFIER
Antibodies		
MPO	Thermo Fisher	Cat. # RB-373-A0, RRID: AB_59598
CALR	Millipore	Cat. # 208912-50UG, RRID: AB_10682608
CALR MUT	Statens Serum Institut, Copenhagen, Denmark	Cat. # 100808
ERp57	Thermo Fisher	Cat. # PA3-009, RRID: AB_2160851)
Peroxidase AffiniPure Goat Anti-Rabbit IgG (H + L)	Jackson Immuno Research	Cat. # 111-035-003, RRID: AB_2313567
Peroxidase AffiniPure Goat Anti-Mouse IgG (H + L)	Jackson Immuno Research	Cat. # 115-035-003, RRID: AB_10015289
MHC-I (PE-conjugated)	Thermo Fisher	Cat. # 12-9983-41, RRID: AB_10545857
CD66b (APC-conjugated)	Ebiosciences	Cat. # 305117
CD15 (BV711-conjugated)	BD Biosciences	Cat. # 563142, RRID: AB_2738026
Biological samples		
Primary granulocytes (see Table 1)	This study	N/A
Chemicals, peptides, and recombinant proteins		
Dulbecco's Modified Eagle's Medium	Thermo Fisher	Cat. # 11965092
Roswell Park Memorial Institute 1640	Thermo Fisher	Cat. # 11875085
jetPRIME®	Polyplos transfection	Cat. # 101000027
PEG-*it*™	System Biosciences	Cat. # LV810A-1
MICROSPIN COLUMNS C18 SILICA	Nest Group Inc	Cat. # NC0194358
Proteinase K from Tritirachium album, lyophilized powder, BioUltra	Sigma-Aldrich	Cat. #P2308
Lysyl Endopeptidase (LysC) for Biochemistry	Wako Pure Chemical Industries	Cat. # 129-02541
Sequencing-grade modified trypsin, frozen	Promega	Cat. #V5113
Critical commercial assays		
Zero Blunt® PCR Cloning Kit	Thermo Fisher	Cat. #K270020
Duolink® Proximity Ligation Assay	Sigma Aldrich	Cat. # DUO92013
Deposited data		
LiP mass spectrometry dataset primary granulocytes	This study	PRIDE database accession number PXD037174
LiP mass spectrometry dataset CMK 11-5 cell lines	This study	PRIDE database accession number PXD037273
Experimental models: Cell lines		
HL-60 CALR^{KO} clone 1 (c.[110_11del; 113del; 117del]/c.[91 + 361T>C; 91 + 362del; 93_113delinsATCCAAACA; 115G>A; 117A>G])	This study	N/A
HL-60 CALR^{KO} clone 2 (c.[94_124 del]/ c.[100_101 AC>GA; 105_106del])	This study	N/A
K42	Prof. Marek Michalak (University Alberta, Alberta)	N/A
MARIMO	Prof. Hitoshi Kiyoi (Nagoya University, Nagoya)	N/A
CMK 11-5 (wildtype and mutant CALR)	Prof. Kazuya Shimoda (University of Miyazaki, Miyazaki)	N/A

(*Continued on next page*)

Continued

REAGENT or RESOURCE	SOURCE	IDENTIFIER
CMK 11-5 CALR^{KO}	Wildschut M. H. E. et al., manuscript in preparation	N/A
Oligonucleotides		
PCWX_CALR_ATTB1_F 5′- GGGGACA AGTTTGTACAAAAAAGCAGGCTTCAC CATGCTGCTATCCGTGCCGCTG-3′	This study	N/A
PCWX_CALR_WT_ATTB1_R 5′- GGGGAC CACTTTGTACAAGAAAGCTGGGTTCTA CAGCTCGTCCTTCTTATCGTCGTC-3′	This study	N/A
PCWX_CALR_MUT_ATTB1_R 5′- GGGGA CCACTTTGTACAAGAAAGCTGGGTTTTA CTTATCGTCGTCGTCCTTGTAGTCG-3′	This study	N/A
PCDNA5_CALR_F 5′-ATATATAAAGC TTGCCACCATGCTGCTATCCGTGCCG-3′	This study	N/A
PCDNA5_CALR_R 5′- ATATATAGCG GCCGCCTACAGCTCGTCCTTGGCC TGGCCGGGGACATCTTC-3′	This study	N/A
PCDNA5_CALR_MUT_R 5′-ATATAT AGCGGCCGCTCAGGCCTCAGTCC AGCCC-3′	This study	N/A
PCDNA5_CALR_MUT_KDEL_R 5′-ATATATAGCGGCCGCTCACA GCTCGTCCTTGGCCTCAGTCCA GCCC-3′	This study	N/A
PCDNA5_CALR_WT_NOKDEL_R 5′- ATATATAGCGGCCGCCTAGGCCTG GCCGGGGACATCTTC-3′	This study	N/A
Recombinant DNA		
pcDNA5-CALRWT	This study	N/A
pcDNA5-CALRMUT-T1	This study	N/A
pcDNA5-CALRMUT-T2	This study	N/A
pcDNA5-CALRMUT-T1-KDEL	This study	N/A
pcDNA5-CALRMUT-T2-KDEL	This study	N/A
pcDNA5-CALRWT-NOKDEL	This study	N/A
pET21-10XHis-CALRWT	This study	N/A
pET21-10XHis-CALRMUT-T1	This study	N/A
pET21-10XHis-CALRMUT-T2	This study	N/A
mEmerald-MPO-N-18	Addgene	Cat. # 54187
Pcwx-UBI-mCHERRY	Dr. Renier Myburgh, Dr. P. Salmon (University of Geneva, Geneva)	N/A
Pcwx-UBI-CALRWT-FLAG-PGK-EGFP	This study	N/A
PCWX-UBI-CALRMUTT1-FLAG-PGK_EGFP	This study	N/A
PCWX-UBI-CALRMUTT2-FLAG-PGK_EGFP	This study	N/A
Software and algorithms		
GraphPad Prism (v9)	GraphPad Software, Inc.).	https://www.graphpad.com
RStudio (v1.2.5042)	RStudio	https://rstudio.com
R (v3.6.1)	R Foundation	https://www.r-project.org
Adobe Illustrator (CS6)	Adobe	https://www.adobe.com
ImageStudio	LI-COR Biosciences	https://www.licor.com/bio/image-studio/
ImageJ	National Institutes of Health	https://imagej.nih.gov/ij/

(*Continued on next page*)

Continued

REAGENT or RESOURCE	SOURCE	IDENTIFIER
FloJo	BD Biosciences	https://www.flowjo.com/
Database for Annotation, Visualization and Integrated Discovery	DAVID Knowledgebase	https://david.ncifcrf.gov/
PyMOL Molecular Graphics System (v2.4)	Schrödinger, LLC	https://pymol.org/
Spectronaut (v11)	Biognosys AG	https://biognosys.com/software/spectronaut
Other		
LCP1 structure (Entry ID 5JOL)	RCSB Protein DataBank	https://www.rcsb.org
LCP1 structure (Entry ID 5JOJ)	RCSB Protein DataBank	https://www.rcsb.org
S100A12 structure (Entry ID 2WC8)	RCSB Protein DataBank	https://www.rcsb.org
S100A12 structure (Entry ID 1E8A)	RCSB Protein DataBank	https://www.rcsb.org
CALR structure (Entry ID 3RG0)	RCSB Protein DataBank	https://www.rcsb.org
PLC structure (Entry ID 6ENY)	RCSB Protein DataBank	https://www.rcsb.org
CYPB structure (Entry ID 3ICI)	RCSB Protein DataBank	https://www.rcsb.org

RESOURCE AVAILABILITY

Lead contact

Further information and requests for resources and reagents should be directed to the lead contact, Alexandre Theocharides (alexandre.theocharides@usz.ch).

Materials availability

The CALR knockout cell lines and plasmids generated from this study are available from the lead contact.

Data and code availability

- The datasets generated in this study have been deposited at PRIDE[1] and are publicly available as of the date of publication. Accession numbers are listed in the key resources table.
- This paper does not report original code.
- Any additional information required to reanalyze the data reported in this paper is available from the lead contact upon request.

EXPERIMENTAL MODEL AND SUBJECT DETAILS

Primary mass spectrometry samples

Granulocytes were isolated from human peripheral blood using Ficoll-Paque PLUS (Cytiva) density gradient centrifugation. 11 ET, 11 MF patient and three age-matched healthy donors (HDs) from the blood donation center (Blutspendedienst Zürich) (Table 1) were included in the study. Written informed consent was obtained from all patients. The study was approved by the local ethics committee (KEK-ZH-NR: 2009-0062/1 and BASEC-NR: 2018-00539). The cohort included individuals aged between 43 and 89 years with a median age of 63 years. The median age and sex composition was comparable between the groups: healthy donors (median age of 60 years and 33.3% female samples); heterozygous *CALR*-mutated (61 years and 45.5%); homozygous *CALR*-mutated (69 years and 33.3%); *JAK2*-mutated (64.5 years and 37.5%).

Cell lines

The K42 mouse embryonic fibroblast cell line, MARIMO cell line, CMK 11-5 cell lines (WT and clone 751),[43] and CMK CALR knockout (KO) cell line were kindly provided by Prof. Marek Michalak (University Alberta, Alberta), Prof. Hitoshi Kiyoi (Nagoya University, Nagoya), Prof. Shimoda (University of Miyasaki, Miyasaki), and Mattheus H. E. Wildschut (unpublished data), respectively. K42 cells were grown in Dulbecco's Modified Eagle's Medium with 10% fetal bovine serum and 1% penicillin-streptomycin (all Thermo Fisher). CALR knockout (CALR KO) HL-60 cell lines were generated using CRISPR-Cas9 and transduced with FLAG-tagged CALR constructs. HL-60 and MARIMO cells were grown in Roswell Park Memorial Institute 1640 with 10% fetal bovine serum and 1% penicillin-streptomycin (all Thermo Fisher).

Generation of *CALR* knockout HL-60 cells

Four CALR exon 2 guide RNAs were designed and complexed with Cas9 according to the manufacturer's protocol yielding ribonucleoprotein complexes (Synthego Gene Knockout Kit, Synthego), which were subsequently transfected into HL-60 cells as described previously.[44] *CALR* knockout clones were confirmed by western blotting. The selected clones were sequenced using the Zero Blunt PCR Cloning Kit (Thermo Fisher) and are outlined in the key resources table.

METHOD DETAILS

DNA plasmids and lentiviral transduction

A plasmid encoding human MPO with a C-terminal Emerald-tag (mEmerald-MPO-N18) was obtained from Addgene (#54187). Human CALR wildtype (WT), type 1 (T1), type 2 (T2), T1/T2 plus C-terminal KDEL sequence were PCR-amplified and subsequently cloned into the pcDNA5/FRT/TO (provided by Dr. N. Chatain, RWTH, Aachen) plasmid using HindIII, NotI restriction sites.[20] To obtain lentiviral constructs with an enhanced green fluorescent protein (eGFP) reporter, eGFP was PCR-amplified from pCLX-UBI-GFP and cloned into pcwx-UBI-PGK-mcherry using AgeI and EcoRV restriction sites yielding pcwx-UBI-PGK-eGFP. Second, CALR WT, T1, and T2 with a C-terminal FLAG tag were cloned into pcwx-UBI-PGK-eGFP by gateway cloning (Invitrogen). The CAG-VAVG, psPAX-2, pCLX-UBI-GFP, and pcwx-UBI-mcherry plasmids were obtained from Dr. R. Myburgh (University Hospital Zurich, Zurich) and Dr. P. Salmon (University of Geneva, Geneva). All Primers are listed in the key resources table. The lentiviral particles were generated using the pcwx-UBI-CALR-PGK-eGFP, psPAX2, CAG-VAVG (MD2G), plasmids and the jetPRIME buffer/reagent (Polyplos transfection). The virus was concentrated using PEG-*it* (System Biosciences). HL-60 CALR KO cells were transduced with pcwx-UBI-CALR-PGK-eGFP in the presence of 10 μg/mL polybrene via spinoculation at 32°C and 800 g for one hour and sorted using fluorescence-activated cell sorting to obtain similar CALR expression levels among transduced clones.

Western blot

Per replica, 20 μg of denatured lysate was stained overnight at 4°C using the following antibodies (key resources table): 1:1000 anti-MPO (Thermo Fisher), 1:5000 anti-CALR (clone FMC75, Millipore) or 1:2000 anti-CALR MUT (i.e., the monoclonal antibody SSI-HYB 285-06 anti-mutated Calreticulin, IgG1/Kappa, clone SSI-4F10 was developed and manufactured by Statens Serum Institut, Copenhagen, Denmark (Cat. # 100808)).[45] The images were developed using horseradish peroxidase–catalyzed chemiluminescence and analyzed using ImageStudio (LI-COR Biosciences).

Proximity ligation assay (PLA)

HL-60 cells expressing CALR or CALR MUT were cultured for 7 h as described above with or without 1 ug/mL of brefeldin A (BFA). Cells were cytospun on glass slides, fixed in PBS with 4% PFA and permeabilized using PBS with 0.2% Triton X-. After blocking in PBS with 10% donkey serum, the primary antibodies were added; anti-CALR 1:100, anti-CALR MUT 1:50, anti-MPO 1:100, and anti-ERp57 (Thermo Fisher) 1:100. The PLA kit was used according to the manufacturer's protocol (Sigma Aldrich) using a DAPI concentration of 1:2000. PLA images were acquired using an LSM 800 microscope (Zeiss), and the maximal signal intensity of the z stack (3 or 5 stacks) was quantified using ImageJ/FIJI software.[46,47]

Flow cytometry

Primary granulocytes and HL-60 cells were fixed and permeabilized as previously described.[23] The following antibodies were used in the study: phycoerythrin-conjugated anti-human MHC-I (clone W6/32, Thermo Fisher), fluorescein-conjugated anti-human MPO (Beckman Coulter), allophycocyanin-conjugated anti-human CD66b (clone G10F5, Biolegend), and brilliant violet 711-conjugated anti-human CD15 (clone W6D3, BD Horizon). Live cells were detected using Zombie Aqua Fixable Viability Kit (Biolegend). The acquisition was performed on a BD LSRFortessa or CantoTM cell analyzer. Data was analyzed using FlowJo™.

Elisa-based binding assay

CALR WT, T1, and T2 were cloned into pET21-10XHis-GST-HRV-dL5 (addgene #73214) using the EcoRI and AgeI restriction, which yielded N-terminally GST-tagged CALR constructs (C-terminal His-tag was excluded) GST-CALR WT, or GST-CALR MUT T1 or T2. Plasmids were expressed in E. coli BL21 DE3. Cells were harvested after growing for 18h at 37°C post IPTG induction (OD^{600} of 0.8, 0.25 mM). Cells were lysed on ice using lysis buffer (50mM HEPES pH 7.5, 300 mM NaCl, 10% glycerol). GST-tagged CALR variants were purified using GST resins (Merck) according to the manufacturer's guidelines and eluted using elution buffer (50mM Tris, 150mM NaCl, pH 8.0 with 10mM reduced glutathione). To test the specificity of each antibody, 20μL of each protein (1μg/mL in PBS) was immobilized on 384-well plates (OptiPlate-384 HB, PerkinElmer) for 2 h at 37°C. After three washes in sample buffer (SB, PBS-Tween (T) 0.1%, 1% SureBlock™), wells were blocked by adding 100μL of blocking buffer (BB, PBS-T 0.1%, 5% SureBlock™) for 1h at room temperature (RT). Primary antibodies were serially diluted in SB and incubated for 1h at RT. 20μL of goat anti-mouse or goat anti-rabbit HRP-coupled secondary antibodies (diluted 1:4000 in SB, Jackson ImmunoResearch) were added to the respective well for 1h at RT. The signal was developed using 20μL TMB (Thermo Fisher), quenched with 20μL 0.5M H_2SO_4, and quantified at 450nm using an EnVision Multimode Plate Reader (PerkinElmer). To assess the binding between CALR variants and MPO, 20μL of GST-CALR variants (1μg/mL in PBS) were immobilized. After blocking and washing, native human MPO (Abcam ref. ab91116, 16 μg/mL in PBS) and MPO-containing HL-60 lysates

(64μg/mL in PBS) were added to CALR-containing wells by serial dilution. After a 2h incubation at 37°C, wells were washed and 20μL of primary anti-MPO antibody (1:1250) was added for 1h at RT.

Limited proteolysis coupled to mass spectrometry (LiP-MS)

Snap frozen pellets from primary granulocytes were resuspended in lysis buffer (20mM HEPES, 150mM KCl, 10mM $MgCl_2$, pH = 7.4, protease inhibitor), lysed by sonication, and centrifuged at 5000g to remove debris. Limited proteolysis was performed as described previously.[26,48] In brief, samples were treated with proteinase K (PK) under controlled conditions (enzyme:substrate ratio of 1:100 for 5min, LiP samples) or with ddH2O (control samples). PK was thermally inactivated at 99°C for 5min. Then, the samples were subjected to complete digestion in denaturing conditions using a sequential digest with LysC and trypsin (1:100 enzyme:substrate). The generated peptides were desalted using C18 columns (The Nest Group Inc.) according to the manufacturer's protocol and analyzed as described previously.[48,49] For data dependent acquisition (DDA) replicates were pooled and LiP and control samples were injected independently. For data independent acquisition (DIA), each replicate a sample was injected.

The DDA spectra were searched against the human Uniprot fasta database (version October 2017) using the SEQUEST HT database search engine (Thermo Fischer Scientific) as described previously.[49] Spectral library generation and targeted data extraction of DIA spectra was performed using the software Spectronaut (Biognosys AG, version 11) with default settings. Cross run normalization of peptide intensities was performed using a global normalization strategy. Differential abundance analysis of protein and peptides was performed using paired student's *t* test and p values were adjusted for multiple testing using the Benjamini-Hochberg method.[50] LiP peptides were considered structurally altered (referred to in text as "structurally altered peptides") if they passed a cut-off of $|FC| > 2$ and q-value <0.05. LiP peptides were corrected for significant underlying protein abundance changes ($|FC| > 1.5$ and q-value < 0.05) as described previously.[26] Glycoproteins, calcium-regulated proteins and the remaining proteins (termed "OTHER") were grouped according to the log2(FC) values into upregulated ($\log2(FC) > 0.585$), unchanged ($0.585 \geq \log2(FC) \geq -0.585$) or downregulated fold change ($\log2(F) < -0.585$) (see dashed line). Proteomic data was analyzed in R (Version 3.6.1).[51–54] Enrichment analysis was performed using the DAVID Functional Annotation Bioinformatics Microarray Analysis tool (https://david.ncifcrf.gov).[55] Structurally altered peptides were mapped to protein structures obtained from the RCSB Protein DataBank (www.rcsb.org) using PyMol (Version 2.4, Schrödinger Inc.). The Protein DataBank Entry IDs of the structures are listed in the key resources table.

QUANTIFICATION AND STATISTICAL ANALYSIS

Western blots, PLA analysis, and elisa-based protein-protein interaction assays consisted of two independent experiments. Statistical analyses were performed with R (R Foundation, version 4.0.3) or GraphPad Prism 9 (GraphPad Software, Inc., version 9). Ordinary ANOVA or Kruskal-Willis tests were performed for multi-group comparisons and Mann-Whitney tests were used for pairwise comparisons. Data is presented as mean ± SD unless otherwise stated. Statistical details are listed in the figure legends.